

Lamb-shift-induced switching of energy transfer in open quantum batteries

Liang Luo¹ and Shun-Cai Zhao^{1,*}

¹*Center for Quantum Materials and Computational Condensed Matter Physics,
Faculty of Science, Kunming University of Science and Technology, Kunming, 650500, PR China*

(Dated: Wednesday 25th March, 2026)

Open quantum batteries (QBs) operate under unavoidable system-environment interactions, where both dissipation and coherent renormalization influence their performance. While most previous studies focus on dissipative effects, the role of environment-induced frequency renormalization, such as the Lamb shift, remains insufficiently explored. In this work, we investigate an externally driven QB composed of two coherently coupled quantum harmonic oscillators, representing the charger and the battery. By incorporating both dissipation and Lamb-shift corrections within a Lindblad master equation, we show that the Lamb shift effectively renormalizes the system eigenfrequencies and thereby modifies the resonance condition with the external drive. We demonstrate that tuning the driving frequency relative to the renormalized eigenmodes leads to a mode-selective energy transfer process, resulting in a controllable redistribution of energy between the charger and the battery. This behavior manifests as a switching of the dominant energy storage channel and can be quantitatively understood through a supermode decomposition of the coupled system. Our results clarify the dynamical role of environment-induced frequency shifts in open quantum batteries and provide a physically transparent framework for optimizing work extraction under realistic operating conditions.

CONTENTS

I. INTRODUCTION	1
II. Model and Theoretical Framework	2
III. Results and Discussion	3
A. Impact of Lamb shift on energy distribution	3
B. Physics Analysis	4
C. Physical interpretation via normal modes	4
D. Experimental Feasibility	5
IV. Conclusion	5
Author contributions	6
V. Acknowledgment	6
References	6

I. INTRODUCTION

Quantum batteries (QBs) represent a cutting-edge frontier in energy storage technology [1–6], promising to revolutionize next-generation quantum devices[7, 8] by leveraging non-classical resources such as coherence[9], entanglement[10], and collective quantum effects [11]. Unlike traditional electrochemical cells, QBs aim to achieve ultrafast charging rates and high power densities by exploiting the unique thermodynamic laws at the microscale [12–14]. The core research motivation lies in developing

efficient and stable quantum energy harvesters capable of powering nanoscale quantum computing and communication networks[15, 16].

The evolution of QB research can be broadly categorized into two stages. Early investigations primarily focused on closed quantum systems[17–19], where the battery’s evolution is assumed to be unitary and isolated from any environment. These studies established the foundational bounds for work extraction and charging power[20–22]. More recently, attention has shifted towards the study of open quantum batteries[23–26], which accounts for the realistic interactions between the system and its surrounding reservoir. Within this context, significant effort has been devoted to mitigating dissipative losses and decoherence effects[27–30]. In continuity with our previous work on the dynamics of open quantum systems [31, 32], we have observed that environmental coupling does more than just induce decay; it fundamentally reshapes the system’s energy landscape.

However, a critical gap persists in the existing literature: the vast majority of prior open-system QB studies[33–37] have failed to consider system-environment interference, effectively neglecting the Lamb shift[38, 39]. By assuming that the environment only induces energy dissipation (represented by decay rates γ_a) without modulating the bare system frequencies (ω_a, ω_b), these models oversimplify the resonance conditions. Such an oversight is particularly problematic in experimental platforms like circuit QED or cavity QED, where vacuum fluctuations inevitably induce frequency shifts [35–37]. Most previous studies have focused on dissipative effects while neglecting coherent renormalization such as the Lamb shift, which may become relevant in precision-controlled platforms.

In this work, we aim to bridge this gap by explic-

* Corresponding author: zsczhao@126.com.

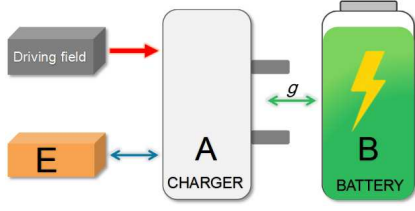


FIG. 1. Schematic of the quantum battery (QB) system. The charger (middle) and battery (right) are quantum harmonic oscillators coupled with strength g (green arrow). The external driving field (left) initiates the charging process (red arrow), while interaction with the environment E leads to both dissipation and an interference-induced shift (blue bidirectional arrow) between the charger and the thermal reservoir.

itly incorporating Lamb-shift corrections into the charging dynamics of an open QB system. We model both the charger and the battery as quantum harmonic oscillators and derive a Lindblad master equation that accounts for both dissipation and the interference-induced frequency renormalization. Unlike prior QB studies that focus solely on the role of decay [40, 41], this paper provides a robust framework to understand how environment-induced energy shifts modify the work-extraction capacity (ergotropy).

Our results reveal a clear manifestation of mode-selective energy transfer governed by the Lamb-shift-modified resonance condition. We demonstrate that by tuning the driving frequency to the renormalized eigenfrequencies λ_{\pm} , one can selectively optimize energy distribution between the charger and the battery—a phenomenon we call the “switching effect.” Furthermore, we propose a frequency correction strategy based on the Lamb-shifted eigenvalues to restore ergotropy that would otherwise degrade due to environmental interference. These findings offer actionable insights for designing controllable quantum energy devices in interference-prone environments.

The remainder of this paper is organized as follows: In Sec. I, we describe the model setup and derive the master equation with Lamb-shift corrections. In Sec. II, we present the numerical results and the physical analysis of the switchable charging dynamics. Finally, the experimental feasibility and conclusions are summarized in Sec. III and Sec. IV.

II. MODEL AND THEORETICAL FRAMEWORK

As schematically illustrated in Fig. 1, we consider an open quantum battery system comprising a *charger* (subsystem A) and a *battery* (subsystem B). Both components are modeled as quantum harmonic oscillators (QHOs) with eigenfrequencies ω_a and ω_b , respectively [42]. The charger is driven by an external laser field with amplitude F and frequency ω_f , while undergoing coherent energy transfer to the battery via a bilinear interaction with coupling

strength g . Throughout this work, we set $\hbar = 1$. Under the dipole and rotating-wave approximations (RWA) [43, 44], the total system Hamiltonian reads

$$\hat{H} = \omega_a \hat{a}^\dagger \hat{a} + \omega_b \hat{b}^\dagger \hat{b} + g (\hat{a} \hat{b}^\dagger + \hat{b} \hat{a}^\dagger) + F (e^{i\omega_f t} \hat{a} + e^{-i\omega_f t} \hat{a}^\dagger). \quad (1)$$

where \hat{a}^\dagger (\hat{a}) and \hat{b}^\dagger (\hat{b}) are the creation (annihilation) operators for the charger and battery, respectively.

We assume the battery is well-isolated, while the charger is coupled to a thermal reservoir, inducing both dissipation and environment-mediated energy shifts. The time evolution of the total density matrix $\hat{\rho}_{AB}$ is governed by the Lindblad master equation [39]:

$$\dot{\hat{\rho}}_{AB} = -i [\hat{H}, \hat{\rho}_{AB}] + \gamma_a (N(T) + 1) \mathcal{D}_{\hat{a}} [\hat{\rho}_{AB}] + \gamma_a N(T) \mathcal{D}_{\hat{a}^\dagger} [\hat{\rho}_{AB}] - i \Delta_L [\hat{a}^\dagger \hat{a}, \hat{\rho}_{AB}], \quad (2)$$

where γ_a is the decay rate and $\mathcal{D}_{\hat{c}}[\hat{\rho}] = \hat{c} \hat{\rho} \hat{c}^\dagger - \frac{1}{2} \{\hat{c}^\dagger \hat{c}, \hat{\rho}\}$ denotes the standard dissipator. The mean thermal excitation number is $N = [\exp(\omega/k_B T) - 1]^{-1}$. Crucially, we incorporate the Lamb shift Δ_L , which originates from the principal value contribution of the system-bath interaction under the Born-Markov and secular approximations. Although often neglected in the weak-coupling limit, Δ_L represents a non-negligible frequency renormalization in realistic open systems, ensuring a physically comprehensive description of the energy-level structure [39].

The dynamical evolution of the expectation value for an arbitrary operator \hat{A} follows the adjoint master equation [45]:

$$\frac{d}{dt} \langle \hat{A} \rangle = -i \langle [\hat{A}, \hat{H}] \rangle + \gamma_a (N(T) + 1) \mathcal{D}[\hat{a}] \langle \hat{A} \rangle + \gamma_a N(T) \mathcal{D}[\hat{a}^\dagger] \langle \hat{A} \rangle - i \Delta_L \langle [\hat{A}, \hat{a}^\dagger \hat{a}] \rangle, \quad (3)$$

where $\mathcal{D}[\hat{O}] \langle \hat{A} \rangle = \langle \hat{O}^\dagger \hat{A} \hat{O} - \frac{1}{2} \{\hat{O}^\dagger \hat{O}, \hat{A}\} \rangle$. In the zero-temperature limit ($N = 0$), the dynamics of the annihilation operators reduce to a set of coupled first-order differential equations [46]:

$$\dot{\langle \hat{a} \rangle} = -i F e^{-i\omega_f t} - i g \langle \hat{b} \rangle - \frac{\Gamma}{2} \langle \hat{a} \rangle, \quad (4a)$$

$$\dot{\langle \hat{b} \rangle} = -i g \langle \hat{a} \rangle - i \omega_b \langle \hat{b} \rangle, \quad (4b)$$

where we have defined the complex decoherence parameter $\Gamma/2 = \gamma_a/2 + i(\omega_a + \Delta_L)$.

To quantify the charging performance, we evaluate the ergotropy—defined as the maximum work extractable from the battery via cyclic unitary operations [47]. For a QHO subsystem initially in the ground state, the instantaneous ergotropy for the charger (W_A) and battery (W_B)

is given by:

$$W_i(t) = E_i(t) - \min_{\hat{U}} \text{Tr}[\hat{H}_i \hat{U} \hat{\rho}_i(t) \hat{U}^\dagger] = \omega_i |\langle \hat{\sigma}(t) \rangle|^2, \quad (5)$$

where $i \in \{A, B\}$ and $\hat{\sigma} \in \{\hat{a}, \hat{b}\}$. Here, $\hat{H}_i = \omega_i \hat{\sigma}^\dagger \hat{\sigma}$ is the free Hamiltonian of the respective subsystem and $\hat{\rho}_i(t)$ is the reduced density matrix. By numerically integrating Eqs. (4) and applying the definitions in Eq. (5), we characterize the energy transfer and storage efficiency of the QB under the influence of environmental interference.

III. RESULTS AND DISCUSSIONS

A. Impact of Lamb shift on energy distribution

In the derivation of the master Eq.(2), the interaction between the system and the reservoir naturally gives rise to a Lamb shift term, denoted as $-i\Delta_L[\hat{a}^\dagger \hat{a}, \hat{\rho}_{AB}]$. This term originates from the environmental vacuum fluctuations and modifies the coherent evolution of the charger mode.

By comparing this contribution with the free evolution term $-i[\omega_a \hat{a}^\dagger \hat{a}, \hat{\rho}_{AB}]$ [45] in the original Hamiltonian (1), we observe that the interaction induces a shift in the *bare frequency* ω_a . To simplify the description of the system's dynamics, we introduce the renormalized frequency defined as:

$$\omega'_a = \omega_a + \Delta_L. \quad (6)$$

Consequently, by absorbing the Lamb shift into the re-defined charger frequency, the effective Hamiltonian of the system can be rewritten in a more concise form:

$$\begin{aligned} \hat{H}' = & \omega'_a \hat{a}^\dagger \hat{a} + \omega_b \hat{b}^\dagger \hat{b} + g (\hat{a} \hat{b}^\dagger + \hat{b} \hat{a}^\dagger) \\ & + F (e^{i\omega_f t} \hat{a} + e^{-i\omega_f t} \hat{a}^\dagger). \end{aligned} \quad (7)$$

This renormalization procedure ensures that the subsequent analysis of the energy transfer and charging power accounts for the environment-induced energy level shifts, providing a more physically accurate representation of the open quantum system.

To facilitate the analysis of the collective excitations, the effective Hamiltonian (7) can be expressed in the matrix representation for two-mode bosonic systems [48]:

$$\hat{H}' = (\hat{a}^\dagger \ \hat{b}^\dagger) \mathbf{G} \begin{pmatrix} \hat{a} \\ \hat{b} \end{pmatrix} + F (e^{i\omega_f t} \hat{a} + e^{-i\omega_f t} \hat{a}^\dagger), \quad (8)$$

where the coupling matrix is defined as $\mathbf{G} = \begin{pmatrix} \omega'_a & g \\ g & \omega_b \end{pmatrix}$. The corresponding eigenfrequencies of the coupled system

are given by the eigenvalues of \mathbf{G} :

$$\lambda_{\pm} = \frac{\omega'_a + \omega_b}{2} \pm \sqrt{\left(\frac{\omega'_a - \omega_b}{2}\right)^2 + g^2}. \quad (9)$$

The physical significance of these eigenvalues becomes evident when considering the optimal charging protocol. In the absence of system-environment interference (i.e., $\Delta_L = 0$), the frequencies reduce to the standard normal mode frequencies $\lambda_{\pm} = \omega \pm g$ (assuming $\omega_a = \omega_b = \omega$), which represent the optimal driving frequencies identified through canonical transformations.

However, the incorporation of the Lamb shift Δ_L inherently shifts these resonance peaks. Under the resonance condition where $\omega_a = \omega_b = \omega$, the shifted eigenvalues(9) become

$$\lambda_{\pm} = \omega + \frac{\Delta_L}{2} \pm \sqrt{g^2 + \left(\frac{\Delta_L}{2}\right)^2}. \quad (10)$$

This shift explains the observed deviation in the battery's energy profile when system-environment interactions are accounted for. Specifically, the optimal driving frequency is no longer determined by the bare system parameters but is reconfigured by the renormalized energy landscape. In the following section, we shall elaborate on the dynamical implications of these shifted eigenvalues.

Weak-coupling regime -To elucidate the impact of the renormalized energy landscape, we analyze the evolution of the charger energy W_A and the battery ergotropy W_B under weak resonant driving ($\omega_f = \lambda_{\pm}$), as shown in Fig. 2. The results reveal a pronounced switching behavior governed by the Lamb shift Δ_L , with the zero-shift point ($\Delta_L = 0$) marking a critical boundary between two distinct dynamical regimes.

This switching originates from the Lamb-shift-induced renormalization of the eigenenergies, which modifies the resonance condition between the driving field and the system. As Δ_L changes sign, the relative alignment between ω_f and the shifted eigenmodes is reversed, leading to a re-configuration of the energy-transfer pathways(See Fig. 2(a) and (c), (b) and (d)).

For $\omega_f = \lambda_-$, a redshift ($\Delta_L < 0$) enhances resonant energy release from the charger(W_A in Fig. 2(a)), yielding faster and more stable output, whereas a blueshift ($\Delta_L > 0$) favors efficient ergotropy accumulation in the battery(W_B in Fig. 2(b)). This inversion follows directly from the exchange of dominant weight between the two normal modes (Comparing W_A in Fig. 2(c), W_B in Fig. 2(d))when the driving frequency is tuned from $\omega_f = \lambda_-$ to $\omega_f = \lambda_+$, demonstrating a mode-dependent flipping of optimal operating conditions.

These results establish the Lamb shift as an effective control knob: by jointly tuning the driving mode and the environment-induced shift, one can selectively optimize either energy discharge or work extraction. This behavior

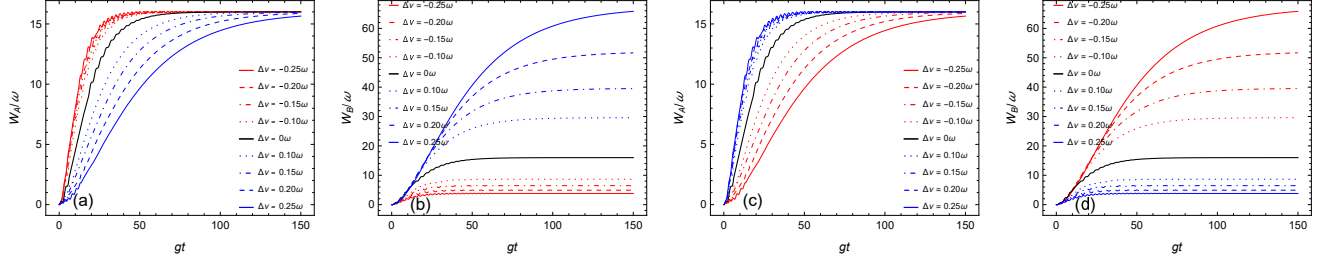


FIG. 2. Evolution of output energy (the charger energy W_A , the battery ergotropy W_B) under weak resonant coupling between charger and quantum battery. Here, $\omega_f = \lambda_-$ for (a) and (b), $\omega_f = \lambda_+$ for (c) and (d), $g = 0.16\omega$, $F = 0.1\omega$, $\gamma_a = 0.05\omega$, and $N(T) = 0$, ω is the scaling unit.

highlights the nontrivial role of vacuum fluctuations in reshaping energy flow in open quantum systems.

Strong-coupling regime- Fig. 3 and 4 present the dynamical evolution of W_A and W_B of the quantum battery under strong coupling ($g = 1.6\omega$), for both resonant (curves in Fig. 3) and off-resonant (curves in Fig. 4 with $\omega_a = \frac{2}{3}\omega_b$) driving conditions. Under resonant strong-coupling driving (curves in Fig. 3), although the switching behavior associated with the redshift and blueshift of the Lamb shift persists, the corresponding contrast is significantly weaker than that observed in the weak-coupling regime in Fig. 2.

In contrast, under off-resonant strong-coupling driving (Fig. 4), both the charger output and the battery ergotropy still exhibit a clear switching effect. However, their dynamics approach steady behavior through pronounced oscillatory patterns.

B. Physics Analysis

In this section, we present the renormalized energy landscape and the resulting switching effect, followed by a detailed physical interpretation using supermode decomposition. To gain insight into the dynamical origin of the switching effect in charger and battery energy, we introduce two supermode operators

$$\begin{aligned}\hat{C}_+ &= \sin \alpha \hat{a} + \cos \alpha \hat{b}, \\ \hat{C}_- &= \cos \alpha \hat{a} - \sin \alpha \hat{b},\end{aligned}\quad (11)$$

with

$$\sin \alpha = \frac{\omega - \lambda_+}{\sqrt{g^2 + (\omega - \lambda_+)^2}}, \quad \cos \alpha = -\frac{g}{\sqrt{g^2 + (\omega - \lambda_+)^2}}.\quad (12)$$

Substituting these into the renormalized Hamiltonian (Eq. (7)) yields a completely decoupled form:

$$\begin{aligned}\hat{H}' &= \lambda_+ \hat{C}_+^\dagger \hat{C}_+ + F \sin \alpha \left(e^{i\omega_f t} \hat{C}_+ + e^{-i\omega_f t} \hat{C}_+^\dagger \right) \\ &+ \lambda_- \hat{C}_-^\dagger \hat{C}_- + F \cos \alpha \left(e^{i\omega_f t} \hat{C}_- + e^{-i\omega_f t} \hat{C}_-^\dagger \right),\end{aligned}\quad (13)$$

where λ_\pm are the eigenfrequencies of the Lamb-shift-corrected coupling matrix G (Eq. (9)). This decomposition shows that the system can be formally regarded as two independent vibrational modes, each driven by a component of the external field.

While the supermode formalism clarifies the distribution of energy between the charger (A) and the battery (B) once a mode is resonantly driven (with the distribution determined by $|\sin \alpha|^2$ and $|\cos \alpha|^2$), it is not the origin of the observed switching effect. The fundamental physical mechanism lies in the Lamb-shift-induced renormalization of the eigenfrequencies:

- The Lamb shift Δ_L modifies the effective eigenfrequencies λ_\pm of the coupled system.
- Changing the sign or magnitude of Δ_L alters the resonance condition between the driving frequency ω_f and the eigenmodes, favoring either charger-dominated or battery-dominated energy extraction.
- The resulting switching in W_A and W_B occurs because the system preferentially absorbs energy through the resonant supermode whose composition favors one subsystem over the other (Fig. 2–4).

Thus, the supermode decomposition serves as a convenient mathematical tool to describe energy partitioning, while the Lamb shift and its impact on resonance provide the physical explanation for the switchable ergotropy observed in the simulations. Explicitly distinguishing these two aspects clarifies the origin of the switching and aligns the discussion with rigorous open quantum system physics.

C. Physical interpretation via normal modes

To further elucidate the mechanism, we diagonalize the coupled system in terms of normal modes. The Hamiltonian can be expressed as two independent modes with frequencies λ_\pm , each driven with an effective amplitude determined by its overlap with the original charger mode.

In this representation, the system dynamics can be understood as follows: the external drive selectively excites

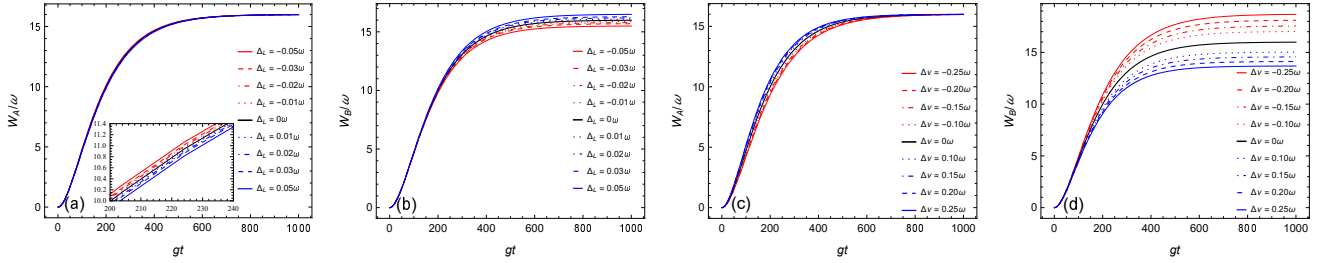


FIG. 3. Evolution of output energy (the charger energy W_A , the battery ergotropy W_B) under strong resonant coupling between charger and quantum battery. Here, $\omega_f = \lambda_-$ for (a) and (b), $\omega_f = \lambda_+$ for (c) and (d), $g = 1.6\omega$, other parameters are the same to Fig.(2) .

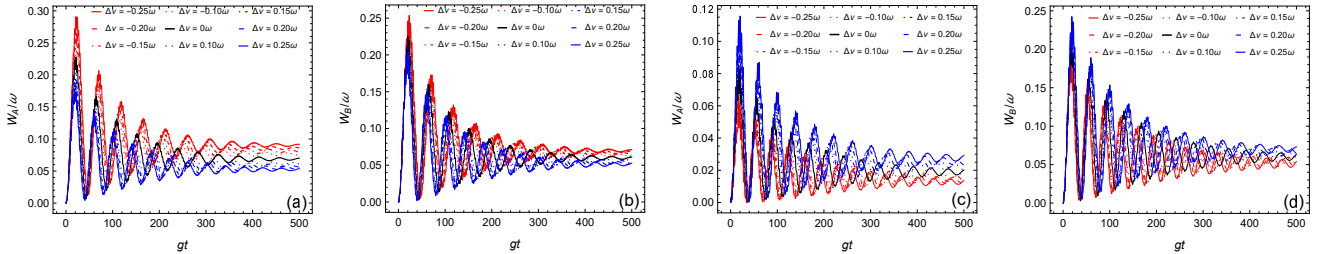


FIG. 4. Evolution of output energy (the charger energy W_A , the battery ergotropy W_B) under nonresonant strong coupling between charger and quantum battery. Here, $\omega_f = \lambda_-$ for (a) and (b), $\omega_f = \lambda_+$ for (c) and (d), $\omega_a = \frac{2}{3}\omega_b$, other parameters are the same to Fig.(3).

one of the normal modes, and the energy distribution between the charger and battery is determined by the composition of that mode.

The Lamb shift modifies the eigenfrequencies and hence shifts the resonance condition. As a result, for a fixed driving frequency, varying Δ_L effectively changes which mode is resonantly excited. This leads to a redistribution of energy between the subsystems, which appears as a switching behavior in the observed quantities.

Therefore, the switching effect can be understood as a consequence of mode-selective excitation in a renormalized energy landscape.

D. Experimental Feasibility

To bridge the gap between our theoretical model and practical implementations, we discuss the experimental feasibility of the proposed switchable ergotropy in state-of-the-art quantum platforms[49]. The coupled quantum harmonic oscillator (QHO) model, described by Eq.(1), can be naturally realized in circuit quantum electrodynamics (circuit QED) architectures, where superconducting resonators or LC circuits act as the charger and battery subsystems[34, 35]. In such systems, the coupling strength g can be engineeringly tuned from the strong coupling regime ($g/\omega \sim 10^{-2}$) to the ultrastrong coupling (USC) regime ($g/\omega > 0.1$) by adjusting the mutual capacitance or inductance between the resonators [36]. These values

directly align with the parameters used in our numerical simulations (e.g., $g = 0.16\omega$ and $g = 1.6\omega$).

Furthermore, the environment-induced Lamb shift Δ_L , which serves as the control knob for the switching effect, is a well-established phenomenon in open quantum systems. In circuit QED, the Lamb shift arises from the coupling between a superconducting qubit or resonator and the vacuum fluctuations of a transmission line or a lossy environment. Experimental observations have reported Lamb shifts as large as 1% to 5% of the transition frequency [37], and even larger shifts are achievable in broadband engineered reservoirs. The renormalized resonance condition $\omega'_a = \omega_a + \Delta_L$ can be precisely probed using standard microwave spectroscopy. Moreover, the driving frequency ω_f of the external laser (or microwave field) is highly tunable in experiments, allowing for the precise targeting of the corrected eigenfrequencies λ_{\pm} . Given the high quality factors of modern superconducting resonators and the ability to engineer system-environment interference, the proposed frequency correction strategy and the resulting switchable energy distribution are well within the reach of current experimental capabilities.

IV. CONCLUSION

In this work, we investigated the impact of the Lamb shift, arising from system-environment interference, on the charging dynamics of open quantum batteries within

a Lindblad framework. We show that the Lamb-shift-induced renormalization of the charger frequency modifies the resonance structure of the coupled system.

By identifying the renormalized eigenfrequencies λ_{\pm} as the correct resonance conditions, we demonstrate that an appropriate frequency correction restores and can further enhance the battery ergotropy. Moreover, we uncover a robust switching effect in energy transfer: tuning the Lamb shift Δ_L and the driving frequency ω_f enables selective control over whether energy is predominantly stored in the battery or retained in the charger, a behavior that persists across different coupling and detuning regimes.

These results establish the Lamb shift as an effective control parameter for optimizing energy transfer in realistic quantum batteries. By bridging the gap between idealized models and dissipative environments, these results provide actionable strategies for engineering high-efficiency quantum energy storage devices. Given the universality of the interference effects discussed here, our framework may be extended to more complex scenarios, includ-

ing non-Markovian dynamics, many-body quantum batteries, and experimental implementations in circuit QED or waveguide-coupled solid-state emitters.

AUTHOR CONTRIBUTIONS

S. C. Zhao conceived the idea and performed the visualization. L. Luo carried out the numerical computations and drafted the manuscript. S. C. Zhao analyzed the results and revised the paper.

V. ACKNOWLEDGMENT

This work is supported by the National Natural Science Foundation of China (Grant Nos. 62065009 and 61565008), Yunnan Fundamental Research Projects, China (Grant No. 2016FB009) and the Foundation for Personnel training projects of Yunnan Province, China (Grant No. KKS201207068).

-
- [1] Z.-G. Lu, G. Tian, X. Y. Lv, and C. Shang, *Phys. Rev. Lett.* **134**, 180401 (2025).
- [2] F. Pirmoradian and K. MÅ_lmer, *Phys. Rev. A* **100**, 043833 (2019).
- [3] W. L. Song, J. L. Wang, B. Zhou, W. L. Yang, and J. H. An, *Phys. Rev. Lett.* **135**, 020405 (2025).
- [4] J. Li and N. Wu, *Phys. Rev. E* **111**, 044118 (2025).
- [5] M.-L. Hu, T. Gao, and H. Fan, *Phys. Rev. A* **111**, 042216 (2025).
- [6] C. Z. Sun, Z. K. Wang, W.-B. Yan, Y. J. Zhang, Z. X. Man, and Q. Y. Cai, *Phys. Rev. A* **112**, 012429 (2025).
- [7] J. Q. Quach, K. E. McGhee, L. Ganzer, D. M. Rouse, B. W. Lovett, E. M. Gauger, J. Keeling, G. Cerullo, D. G. Lidzey, and T. Virgili, *Science Advances* **8**, eabk3160 (2022).
- [8] Z. Y. Peng, S. C. Zhao, L. Luo, and N. Y. Zhuang, *Physica A: Statistical Mechanics and its Applications* **689**, 131462 (2025).
- [9] F. H. Kamin, F. T. Tabesh, S. Salimi, and A. C. Santos, *Phys. Rev. E* **102**, 052109 (2020).
- [10] K. Sen and U. Sen, *Phys. Rev. A* **104**, L030402 (2021).
- [11] F. Mayo and A. J. Roncaglia, *Phys. Rev. A* **105**, 062203 (2022).
- [12] F. Cleri, *arXiv* (2024), [arXiv:2404.09663](https://arxiv.org/abs/2404.09663) [quant-ph].
- [13] M. Aguilar and E. Lutz, *Science Advances* **11**, eadw8462 (2025).
- [14] P. P. Potts, *arXiv* (2019), [arXiv:1906.07439](https://arxiv.org/abs/1906.07439) [quant-ph].
- [15] F. Campaioli, F. A. Pollock, F. C. Binder, L. CÅ_leri, J. Goold, S. Vinjanampathy, and K. Modi, *Phys. Rev. Lett.* **118**, 150601 (2017).
- [16] D. Ferraro, M. Campisi, G. M. Andolina, V. Pellegrini, and M. Polini, *Phys. Rev. Lett.* **120**, 117702 (2018).
- [17] H. L. Shi, S. Ding, Q. K. Wan, X. H. Wang, and W. L. Yang, *Phys. Rev. Lett.* **129**, 130602 (2022).
- [18] T. P. Le, J. Levinsen, K. Modi, M. M. Parish, and F. A. Pollock, *Phys. Rev. A* **97**, 022106 (2018).
- [19] Y. Y. Zhang, T.-R. Yang, L. Fu, and X. Wang, *Phys. Rev. E* **99**, 052106 (2019).
- [20] R. Alicki and M. Fannes, *Phys. Rev. E* **87**, 042123 (2013).
- [21] A. C. Santos, B. Å_akmak, S. Campbell, and N. T. Zinner, *Phys. Rev. E* **100**, 032107 (2019).
- [22] G. M. Andolina, M. Keck, A. Mari, V. Giovannetti, and M. Polini, *Phys. Rev. B* **99**, 205437 (2019).
- [23] Y. Yao and X. Q. Shao, *Phys. Rev. E* **104**, 044116 (2021).
- [24] S. Pokhrel and J. Gea-Banacloche, *Phys. Rev. Lett.* **134**, 130401 (2025).
- [25] S. Zakavati, F. T. Tabesh, and S. Salimi, *Phys. Rev. E* **104**, 054117 (2021).
- [26] F. T. Tabesh, F. H. Kamin, and S. Salimi, *Phys. Rev. A* **102**, 052223 (2020).
- [27] J. Q. Quach and W. J. Munro, *Phys. Rev. Appl.* **14**, 024092 (2020).
- [28] V. Abakumova and S. Lyakhovich, *Annals of Physics* **453**, 169322 (2023).
- [29] F. Barra, *Phys. Rev. Lett.* **122**, 210601 (2019).
- [30] D. Gaspard and J.-M. Sparenberg, *Phys. Rev. A* **107**, 022214 (2023).
- [31] S. Q. Zhong, S. C. Zhao, and S. N. Zhu, *Results Phys.* **24**, 104094 (2021).
- [32] S. N. Zhu, S. C. Zhao, L. J. Chen, and Q. Fang, *The European Physical Journal Plus* **138**, 1053 (2023).
- [33] G. Aruldhas, *Quantum Mechanics*, 2nd ed. (Prentice-Hall of India Pvt. Ltd., 2009) Chap. 15.15, p. 404.
- [34] M. Gross and S. Haroche, *Physics Reports* **93**, 301 (1982).
- [35] A. Blais, A. L. Grimsmo, S. M. Girvin, and A. Wallraff, *Rev. Mod. Phys.* **93**, 025005 (2021).
- [36] P. Forn-DÅ_az, L. Lamata, E. Rico, J. Kono, and E. Solano, *Rev. Mod. Phys.* **91**, 025005 (2019).
- [37] A. Fragner, M. GÅ_ppel, J. M. Fink, M. Baur, R. Bianchetti, P. J. Leek, A. Blais, and A. Wallraff, *Science* **322**, 1357 (2008).

- [38] W. E. Lamb and R. C. Retherford, *Phys. Rev.* **72**, 241 (1947).
- [39] H. P. Breuer and F. Petruccione, *The Theory of Open Quantum Systems* (Oxford University Press, 2007).
- [40] H. A. Bethe, *Phys. Rev.* **72**, 339 (1947).
- [41] S. Yang, H. Zheng, R. Hong, S. Y. Zhu, and M. S. Zubairy, *Phys. Rev. A* **81**, 052501 (2010).
- [42] G. M. Andolina, D. Farina, A. Mari, V. Pellegrini, V. Giovannetti, and M. Polini, *Phys. Rev. B* **98**, 205423 (2018).
- [43] R. Loudon, *The Quantum Theory of Light* (Oxford University Press, 2000).
- [44] S. C. Zhao, Z. R. Zhao, and N. Y. Zhuang, *Phys. Rev. E* **112**, 024129 (2025).
- [45] H. J. Carmichael, Lecture 1- master equations and sources i, in [An Open Systems Approach to Quantum Optics](#), Lecture Notes in Physics: New Series m: Monographs (Springer-Verlag, Berlin, Heidelberg, 1993) Chap. 1, pp. 6–21.
- [46] D. Farina, G. M. Andolina, A. Mari, M. Polini, and V. Giovannetti, *Phys. Rev. B* **99**, 035421 (2019).
- [47] A. E. Allahverdyan, R. Balian, and T. M. Nieuwenhuizen, *Europhys. Lett.* **67**, 565 (2004).
- [48] D. H. Wu and V. V. Albert, *Physics Letters A* **422**, 127779 (2022).
- [49] R. Upadhyay, G. Thomas, Y. C. Chang, D. S. Golubev, A. Guthrie, A. Gubaydullin, J. T. Peltonen, and J. P. Pekola, *Phys. Rev. Appl.* **16**, 044045 (2021).